HHS Public Access

Author manuscript

J Mol Biol. Author manuscript; available in PMC 2017 November 06.

Published in final edited form as:

J Mol Biol. 2016 November 6; 428(22): 4503–4519. doi:10.1016/j.jmb.2016.09.016.

An Adaptive mutation in *Enterococcus faecium* LiaR Associated with Antimicrobial Peptide Resistance Mimics Phosphorylation and Stabilizes LiaR in an Activated State

Milya Davlieva[1], **Angel Tovar-Yanez**[1], **Kimberly DeBruler**[1], **Paul G. Leonard**[2], **Michael R. Zianni**[3], **Cesar A. Arias**[4,5,6], and **Yousif Shamoo**[1]

[1]Department of Biosciences, Rice University, Houston, TX 77005 USA

[2]Core for Biomolecular Structure and Function, Department of Genomic Medicine, The University of Texas MD Anderson Cancer Center, Houston, TX, USA

[3]Plant-Microbe Genomics Facility, The Ohio State University, Columbus, OH, USA

[4]UTHealth Center for Antimicrobial Resistance and Bacterial Genomics, Department of Internal Medicine, University of Texas Medical School at Houston, Houston, TX, USA

[5]Department of Microbiology and Molecular Genetics, The University of Texas Health Science Center at Houston, Houston, TX, USA

[6]Molecular Genetics and Antimicrobial Resistance Unit, International Center for Microbial Genomics, Universidad El Bosque, Bogota, Colombia

Abstract

The cyclic antimicrobial lipopeptide daptomycin triggers the LiaFSR membrane stress response pathway in enterococci and many other Gram-positive organisms. LiaR is the response regulator that, upon phosphorylation, binds in a sequence specific manner to DNA to regulate transcription in response to membrane stress. In clinical settings, nonsusceptibility to daptomycin by *Enterococcus faecium* is correlated frequently with a mutation in LiaR of Trp73 to Cys ($LiaR^{W73C}$). We have determined the structure of the activated *Enterococcus faecium* LiaR protein at 3.2 Å resolution and, in combination with solution studies, show that activation of LiaR induces formation of a LiaR dimer that increases LiaR affinity at least 40-fold for the extended regulatory regions upstream of the *liaFSR* and *liaXYZ* operons. *In vitro*, $LiaR^{W73C}$ induces phosphorylation-

Accession numbers

Structure factors and final atomic coordinates have been deposited with the Protein Data Bank (PDB ID: **5HEV**)

Conflict of interest

Dr. Cesar Arias is on the speaker's Bureau for Forest, Theravance, Pfizer, Astra-Zeneca, Cubist, The Medicines Company, Norvartis. He is also consulting for Theravance, Cubist, Bayer and grant investigator for Theravance and Scientific advisor (review panel or advisor committee) for Bayer.

Authors Contributions

MD, CAA and YS designed research, analyzed data, and wrote the paper; MD, AT-Y, KD, PGL, and MRZ performed the experiments. PGL edited the manuscript.

independent dimerization of LiaR and provides a biochemical basis for non-susceptibility to daptomycin by upregulation of the LiaFSR regulon. A comparison of the *Enterococcus faecalis* LiaR, *Enterococcus faecium* LiaR and the LiaR homolog from *Staphylococcus aureus* (VraR) and the mutations associated with daptomycin resistance suggest that physicochemical properties such as oligomerization state and DNA specificity, though tuned to the biology of each organism, share some features that could be targeted for new antimicrobials.

Graphical abstract

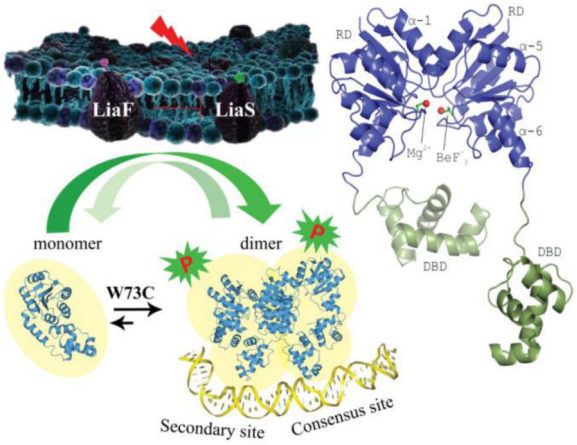

Keywords

LiaR; *E. faecium*; Response regulator; Daptomycin resistance; X-ray

Introduction

The continuing rise and persistence of multi-drug resistant pathogens poses substantial burdens on the clinical community. Vancomycin-resistant enterococci (VRE) are a leading cause of Hospital-Associated Infections (HAI) and are among the most recalcitrant nosocomial pathogens. VRE often develop resistance to a variety of antibiotics making the treatment of infections challenging [1]. In particular, *E. faecium* is the most multidrug-resistant of the enterococcal species affecting critically ill patients. Indeed, the Infectious Diseases Society of America (IDSA) has included *E. faecium* as one of the “no-**E**SKAPE” pathogens [2], against which new drugs are urgently needed. With therapeutic options dwindling, the cyclic lipopeptide daptomycin (DAP) has become one of the last remaining bactericidal options for the treatment of multi-drug resistant enterococcal infections. Unfortunately, the clinical efficacy of DAP is being challenged by the development of resistance which tends to emerge during therapy [3-5].

Daptomycin is a cyclic lipopeptide that targets the cell membrane of Gram-positive bacteria in a calcium-dependent manner becoming a *de facto* cationic antimicrobial peptide [6]. Recent studies have suggested that the association of the calcium-daptomycin complex to the bacterial cell membrane depends on the presence of phosphatidylglycerol-rich regions in the outer leaflet of the cell membrane with a marked preference for the septa of dividing

cells [7]. Upon insertion into the membrane, daptomycin disrupts membrane homeostasis leading to rapid cell death [7-9].

Studies using *Bacillus subtilis*, enterococci and methicillin-resistant *Staphylococcus aureus* have suggested that daptomycin disrupts membrane potential via leakage of small ions such as intracellular potassium resulting in alterations in cell physiology and cell division [7, 10-12]. The biochemical mechanism for DAP resistance is still under investigation but it is apparent that there are distinct phenotypic differences associated with the emergence of daptomycin non-susceptibility between *E. faecium, E. faecalis* and *S. aureus* [6, 7, 13]. To date, there are at least two distinct biochemical mechanisms for cells to reduce their susceptibility to daptomycin. In *S. aureus* and *B. subtilis* changes in the cell envelope appear to increase the overall positive charge of the cell surface, repelling the antibiotic from the membrane target ('repulsion') [6, 14, 15]. In contrast, in *E. faecalis* there is evidence for a 'diversion' mechanism in which DAP is diverted away from the division septa [6, 16, 17]. In the case of *E. faecium,* higher levels of daptomycin resistance appear to be associated more strongly with the repulsion mechanism while strains of *E. faecium* that are susceptible to lower concentrations seem to be able to divert the antibiotic molecule, suggesting that molecular strategies for resistance between species is more complex than may have been anticipated [16, 17]. One of the most important mediators of daptomycin resistance in enterococci is the three-component LiaFSR signaling pathway [6, 16, 18]. Activation of this system triggers an adaptive response to the antibiotic attack by leading to downstream changes in the transcription of several operons, such as *liaFSR* and *liaXYZ* to alter membrane homeostasis resulting in resistance to DAP and antimicrobial peptides [18, 19]. The *liaFSR* operon encodes LiaS, a membrane bound kinase; LiaF, a protein suggested to inhibit LiaS phosphorylation activity in the absence of membrane stress; and LiaR, a response regulator that is phosphorylated by LiaS to alter transcription from the LiaR regulon. Deletion of *liaR* in both *E. faecalis* and *E. faecium* abolishes the adaptive response and restores susceptibility to daptomycin and antimicrobial peptides, supporting the pivotal role of LiaR in the mechanism of resistance [16]. LiaR is comprised of two functional domains: a receiver domain (residues 1-139) that can be phosphorylated and a DNA binding domain (residues 140-210) with a Helix-Turn-Helix motif that recognizes specific regulatory DNA sequences via formation of a DNA binding domain dimer. Recently, we demonstrated that activation of LiaR in *E. faecalis* (*Efc* LiaR) promotes formation of a LiaR tetramer that allows LiaR to recognize complex upstream regulatory regions that extend beyond the predicted consensus sequence. Additionally, we showed that an adaptive mutation isolated in response to DAP exposure (*Efc* $\text{LiaR}^{\text{D191N}}$) "hyperactivates" the *liaFSR* system leading to resistance [19]. Interestingly, emergence of daptomycin resistance in clinical isolates of *E. faecium* is highly associated with a Trp73 to Cys substitution in LiaR (*Efm* $\text{LiaR}^{\text{W73C}}$) [17]. Recently published whole genome sequence analysis of 19 *E. faecium* clinical isolates with DAP MICs between 3 to 32 μg/ml indicate that a Trp73 to Cys substitution in response regulator LiaR was the most frequent change in epidemiologically unrelated clinical isolates of *E. faecium* with DAP MICs ≥ 3 μg/ml. *Efm* $\text{LiaR}^{\text{W73C}}$ is typically found with a second mutation in the kinase $\text{LiaS}^{\text{T120A}}$ suggesting a potential epistatic relationship [17].

A critical difference between the *Efc* $\text{LiaR}^{\text{D191N}}$ and *Efm* $\text{LiaR}^{\text{W73C}}$ is that the "triggering" mutations associated with daptomycin non-susceptibility are located in different domains of

the protein, suggesting that the mechanism of activation associated with LiaR substitutions in DAP resistant clinical strains may differ between *E. faecalis* and *E. faecium.*

Using a combination of biophysical and structural approaches we were able to compare and contrast the molecular details of the adaptive mutations that lead to decreased daptomycin susceptibility in *E. faecalis* and *E. faecium*. We show that in the absence of phosphorylation, *Efm* LiaR exists predominately as a monomer and that activation with the chemical phosphomimic BeF_3^- strongly favors formation of a dimer with high affinity for extended DNA recognition sequences. This finding contrasts with our earlier study of *Efc* LiaR in which the protein undergoes a dimer to tetramer transition upon phosphorylation [19]. Taken together, our results show that while there are similarities between *E. faecium* LiaR, *E. faecalis* LiaR and the LiaR homolog VraR of *S. aureus*, there are substantial and consequential physicochemical differences. New small molecules that might target LiaR to suppress the membrane stress response of these organisms and thereby extend the efficacy of DAP or other membrane damaging agents should be thoughtfully directed at the common molecular attributes of LiaR and the LiaR homolog VraR to have the broadest applicability.

Results

Beryllofluoride (BeF_3^-) stabilizes *E. faecium* LiaR as a dimer

Phosphorylation-dependent oligomerization and consequent activation of response regulators can vary widely between organisms. Based on a comparison of the *E. faecium* LiaR sequence with that of *E. faecalis* LiaR and other response regulators from NarL/FixJ subfamily, such as *S. aureus* VraR, *B. subtilis* LiaR, *E. coli* NarL, FixJ, Asp-54 was identified as a potential site for phosphorylation [19, 20].

To elucidate the changes in quaternary structure associated with phosphorylation, we used Beryllium trifluoride (BeF_3^-) binding to LiaR as a functional mimic for phosphorylation [21]. BeF_3^-, made *in situ,* is a simple and general method to reproduce a stable phosphorylated-like state [22]. Using sedimentation equilibrium analytical ultracentrifugation (SEQ), we determined the oligomerization state of full length *Efm* LiaR as well as the isolated receiver domain (residues 1-139 and referred to hereafter as $LiaR^{RD}$) with and without BeF_3^- and the DNA binding domain (residues 140-210 and referred to hereafter as $LiaR^{DBD}$) (Figure 1, S1). Interestingly, the oligomerization of the full-length *Efm* LiaR differs both qualitatively and quantitatively from what we reported previously for *E. faecalis* LiaR [19]. Our analytical ultracentrifugation studies suggest that inactivated *Efm* LiaR exists nearly exclusively as monomer in solution with a dissociation constant of K_d >1600 μM and that addition of BeF_3^- promotes dimer formation (K_d = 15 μM) (Table 1). We estimated that the propensity towards dimerization is increased at least 2 orders of magnitude by the formation of the BeF_3^-:LiaR complex. Activation of *Efm* LiaR by BeF_3^- produces a monomer↔dimer transition with no observable higher order oligomers like tetramers. To confirm these results we also performed a sedimentation velocity analytical ultracentrifugation experiment with solutions containing 50 μM *Efm* LiaR or 5 μM *Efm* LiaR respectively. The sedimentation velocity data was interpreted using a local continuous distribution model searching for species corresponding to 0.5 to 15 Svedbergs. Using this model, we observe two main species with sedimentation coefficients of 1.4 S and 2.0 S

respectively. These two species have apparent molecular weights of 23.3 kDa and 40.9 kDa respectively, suggesting the two peaks represent monomeric and dimeric populations of LiaR (Figure S2). By integrating the peaks in the c(S) distribution separately we estimate the fraction of LiaR that is present as a homodimer in the 5 μM and 50 μM samples to be 0% and 11% respectively, providing further evidence that unphosphorylated *Efm* LiaR has only a very weak propensity to dimerize.

To further characterize the behavior of *Efm* LiaR in solution, we also analyzed the contribution of isolated LiaR domains to oligomerization in the presence and absence of BeF_3^-. Sedimentation equilibrium analysis of the domains in the absence of BeF_3^- showed a weak but detectable propensity for dimerization by the *Efm* $LiaR^{RD}$ (K_d = 676 μM) and a much stronger dimerization propensity for the *Efm* $LiaR^{DBD}$ (K_d = 0.4 μM). Addition of BeF_3^- increased the extent of dimerization formation of *Efm* $LiaR^{RD}$ by a remarkable 198-fold to a K_d of 3.4 μM. These analyses indicate that while DNA binding domain is capable of homodimerization (K_d = 0.4 μM), the oligomerization of the *Efm* $LiaR^{RD}$ is strongly dependent on phosphorylation, consistent with a regulatory role *in vivo*.

$LiaR^{W73C}$ from a daptomycin-resistant clinical isolate of *E. faecium* promotes phosphorylation-independent dimerization of the LiaR protein

Having established that phosphorylation controls a monomer↔dimer transition for the wild-type *Efm* LiaR, we sought to investigate whether the substitution of Trp73 to Cys in LiaR (the most common LiaR change associated with daptomycin resistance in *E. faecium* clinical isolates) [17, 23] has a direct effect on LiaR oligomerization. Using sedimentation equilibrium experiments of the full length *Efm* $LiaR^{W73C}$ and receiver domain alone (*Efm* $LiaR^{(RD)W73C}$) in the presence and absence of BeF_3^-, we showed that the W73C substitution promotes phosphorylation-independent dimerization of *Efm* LiaR. Indeed, as mentioned above, in the absence of BeF_3^- we were unable to measure any significant dimerization of the full length *Efm* LiaR. In contrast, *Efm* $LiaR^{W73C}$ showed a readily detectable level of dimerization (K_d=182 μM), suggesting that the Trp73 to Cys substitution strongly stimulates phosphorylation-independent dimerization. This phenomenon was further confirmed by our studies on *Efm* $LiaR^{(RD)W73C}$ which showed a 7-fold higher propensity for dimerization compared to the wild type *Efm* $LiaR^{RD}$. The higher propensity to form a dimer was also observed by sedimentation velocity analytical ultracentrifugation (Figure S3). Using a local continuous c(S) distribution model we could interpret the relative size of the populations of monomer, dimer and larger oligomeric species for the 50 μM and 5 μM samples tested. In agreement with the sedimentation equilibrium results, we observed a greater proportion of the protein in the homodimer state for the W73C mutant of LiaR, relative to the wild type protein. For the 50 μM protein sample 59% of the total protein had a sedimentation coefficient of 1.8 S corresponding to monomeric LiaR (apparent MW of 27 kDa). 34% of the total protein is the homodimer form with a sedimentation coefficient of 2.8 S and apparent MW of 48 kDa. We additionally observed a small fraction of the protein at larger sedimentation coefficients of 4.2 S, 5.5 S and 6.6 S and with apparent molecular weights of 90 kDa, 134 kDa, or 178 kDa respectively that total 8% of the protein population in the 50 μM. These apparent molecular weights correspond to tetramer, hexamer and octamer species of LiaR suggesting the W73C mutation can promote the formation of larger

species. As we did not observe these species by size exclusion chromatography it is unclear if these are non specific aggregation effects or a biologically relevant species that might exist in *E. faecium*. Gel filtration studies further corroborate our finding that *Efm* LiaR^{W73C} promotes formation of a phosphorylation independent dimer (Supplementary Information, S4).

Interestingly, and unlike the wild type protein, we could not detect any further increase in dimerization of the full length *Efm* LiaR^{W73C} in the presence of BeF_3^-. Instead, the best fit for dimerization was with a K_d of 236 μM, which is similar to the dimerization constant observed for *Efm* LiaR^{W73C} in the absence of BeF_3^-. This finding is consistent with a model in which the mutation of Trp-73 to cysteine has effectively stimulated the formation of the activated LiaR dimer to the same extent as phosphorylation. It is also possible that the increased propensity for dimerization leads to an increased efficiency of phosphorylation by LiaS. Thermal denaturation studies show that *Efm* LiaR^{W73C} is 4.7 °C less stable than wild type consistent with a model in which the adaptive mutation has potentially destabilized contacts between the receiver and DNA binding domains (Supplementary Information, S5).

When we tested the effect of BeF_3^- on the receiver domain alone (*Efm* LiaR$^{(RD)W73C}$), we observed a marked increase in dimerization. Indeed, the K_d of dimerization for *Efm* LiaR$^{(RD)W73C}$ increased from 94 to 0.8 μM. Our results suggest that the DNA binding domain may also have a role in determining the extent of dimerization induced by either phosphorylation or the presence of BeF_3^-. Thus, in the absence of the DNA binding domain, the extent of dimerization is further enhanced by BeF_3^- in a manner that is not observed for the intact protein.

The crystal structure of full length *Efm* LiaR is a dimer poised to make interactions with its target DNA

We determined the X-ray crystal structure of *Efm* LiaR in the beryllofluoride-activated state to reveal information about the conformational changes induced by phosphorylation. Response regulators have been classified into several common types including the NarL-type that includes a common helix-turn-helix (HTH) motif, OmpR-type that includes a winged HTH motif, Spo0A-type, and Fis-like [24]. The structure of *Efm* R494 LiaR suggests that this protein belongs to the NarL/FixJ subfamily of proteins [20, 24].

The *Efm* LiaR:BeF_3^- structure contains four protomers in the asymmetric unit each with a BeF_3^- bound to the predicted phosphorylation site at Asp54 (Figure 2, S6). Essentially, a pair of activated dimers are observed in the asymmetric unit. Based on homology to other NarL-type response regulators residue Thr-82 and aromatic residue Tyr-101 would be predicted to play a direct role in the activation mechanism through their hydroxyl groups **[25].** In the *Efm* LiaR:BeF_3^- structure residues Thr82 and Tyr101 are oriented toward the predicted phosphorylation site, adopting inward positions consistent with BeF_3^- stimulated formation of the active phosphorylated state (Figure 3). Within the active site, BeF_3^- is stabilized by a single Mg^{2+} ion and the backbone amide of Val56. Previous studies have suggested that the residue equivalent to Val56 is one of the structural determinants that influence the auto-dephosphorylation rate of response regulator proteins [26, 27]. BeF_3^- is also in a position to make hydrogen bonds to Thr82 and Ser83 and a salt bridge to Lys104

(Figure 3a,b). As shown in Figure 2, each protomer has a canonical regulatory domain fold with the $(\beta\alpha)_5$ arrangement and Helix-Turn-Helix DNA binding domain seen in other NarL-like proteins [20, 24, 25].

Helix α-6 followed by short loop creates a flexible linker between the receiver and DNA-binding domains. Interestingly, the arrangement of the DNA binding domains is substantially different from the activated form of *S. aureus* VraR. Presumably this reflects the mobility of the DNA binding domains in both structures when DNA is not present. Our BeF_3^- activated structure is consistent with full-length *Efm* LiaR poised in a configuration to interact with DNA. Two of the four DNA binding domains observed in our structure are extended well away from the receiver domain dimer and illustrate the conformational flexibility of the linker regions that join them to the domain (Figure 2).

In the *Efm* LiaR:BeF_3^- co-structure, two receiver domain dimers (indicated as chains A-F and B-C respectively) are observed in the asymmetric unit (Figure 4a-b). The major interaction surface between neighboring receiver domains buries ~1034 $Å^2$ of solvent accessible surface area through the α4-ß5-α5 interfaces. The protein-protein interactions of the two receiver domains involves 3 potential salt bridges and 3 hydrogen bonds that were also observed in the *S. aureus* response regulator VraR [19] and are presumed to stabilize the quaternary structure. Like *Efm* LiaR, *S. aureus* VraR crystallized as two pairs of receiver domain dimers (Figure 4c-d). In the case of VraR, the DNA binding domains formed additional dimer interfaces but not between the two proteins that comprise the receiver domain dimer but rather as a domain swap (Figure 4d). In the *Efm* LiaR:BeF_3^- co-structure, each DNA binding domain also formed additional dimer interfaces (Figure 4e-f) but with DNA binding domains contributed from symmetry related molecules and not to the one that is contributed by the proximal LiaR protomer that comprises the LiaR:LiaR dimer (a domain swap). Thus, the domain swap in the activated VraR tetramer structure and *Efm* LiaR:BeF_3^- co-structure are very different and may reflect flexibility of linker regions that join the DNA binding domains to the receiver domain[28]. The arrangement of the *Efm* LiaR:BeF_3^- DNA binding domains is likely to be a crystal packing artifact but shows that DNA binding domains can explore a very large volume, a feature that may be important to binding the large extended DNA at the promoter.

The phosphorylation-triggered dimerization surface of *E. faecium* LiaR is similar to that of *S. aureus* VraR

The receiver domain of *Efm* LiaR forms a dimer that associates through a hydrophobic interface comprised of α1-α5 that buries 692 $Å^2$ (Figure 3a,c). This dimerization interface, lined by hydrophobic amino acids Val13, Val17, Ser19, Tyr20, Lys104, Ala108 is similar to those found in the structures of *B. subtilis* DesR [27] and VraR [28] suggesting that these interfacial residues are well conserved among members of NarL subfamily.

Earlier studies have shown that phosphorylation promotes dimerization through different surfaces among different response regulators. While members of the PhoB/OmpR family [29, 30] and FixJ [28, 31] utilize the hydrophobic surface of the α4-β5-α5 interface for phosphorylation triggered dimerization, the NarL transcription factor from *E. coli* [32], the cell-density-responsive transcription factor LuxR from *S. aureus, S. aureus* VraR [28] and *B.*

subtilis DesR [27] employ a novel α1-α5 contact surface. An analogous involvement of helix α1 in intermolecular contacts has also been established in the *M. tuberculosis* NarL [33] and *E.coli* UhpA [34].

In the VraR structure it has been suggested that movement of α-6 is part of the activation mechanism in which the angle of the helix α-6 changes by 35° in response to phosphorylation [28]. To determine whether the interface for the α-6 helices packing against each other is conserved between VraR and *Efm* LiaR after activation, we superimposed the receiver domain structures of the two proteins. Based on this analysis, we concluded that the dimerization interaction is similar between *S. aureus* VraR and *E. faecium* LiaR with an overall root mean square deviation (r.m.s.d.) of 1.14 Å. [35].

Efm LiaR DNA recognition motifs upstream of the putative promoters for both the *Efm liaFSR* and the *liaXYZ* operons are comparable in size and organization to those of *E. faecalis*

Our previous studies revealed that *Efc* LiaR recognizes an extended stretch of DNA that extends beyond the proposed canonical consensus sequence $T(X)_4C(X)_4G(X)_4A$, suggesting a more complex level of regulatory control for target operons [19]. We previously showed that in *E. faecalis* such consensus sequences are present upstream of the *liaFSR* and *liaXYZ* operons [19]. Inspection of the 5' region of the *Efm liaXYZ* and *liaFSR* operons revealed three and four potential consensus sites, respectively. We used DNA Footprint Analysis by Automated Capillary Electrophoresis (DFACE) to identify the DNA sequences protected by activated *Efm* LiaR. Our initial studies indicated that the unphosphorylated *Efm* LiaR protein had no measurable affinity for the DNA upstream of either operon. In contrast, when *Efm* LiaR is activated by formation of the *Efm* LiaR:BeF_3^- complex, protection of DNA across extended regions of DNA upstream of the *liaXYZ* and *liaFSR* operons could be identified readily. We mapped the LiaR binding region from −292 to +65 for *liaXYZ* and −281 to +98 for *liaFSR*. The BeF_3^- activated protein revealed a concentration dependent region of protection for both operons with no observable protection at 0.5 μM, slight protection at 2.5 μM, (data not shown) and significant protection at 5.0 μM and 50 μM protein (Figure 5a, c). The 50 μM *Efm* LiaR concentration had a slight increase in protection and cleavage at most bases as compared to 5.0 μM. Interestingly, *Efm* LiaR protects only one canonical binding motif of $T(X)_4C(X)_4G(X)_4A$ for both operons. As shown in Figure 5, the consensus binding regions starting at positions −80 and −62 respectively for *liaXYZ* and *liaFSR* are protected by the *Efm* LiaR:BeF_3^- complex. The other potential consensus binding sites did not show protection (data not shown).

While both *liaFSR* and *liaXYZ* show binding at a single consensus binding sequence, the overall organization of the protected regions with respect to each other is very different. Based on sequence homology to other response regulators containing a canonical helix-turn-helix DNA binding motif, the active species of *Efm* LiaR would be expected to dimerize and have site size of ~21 nucleotides. In contrast, the contiguous protection site for the *Efm liaXYZ* promoter extends from position −120 to −75 (about 45 bp) and includes the predicted consensus region (−95 to −80) and nucleotides from −96 to −120. We refer to this additional region outside the consensus sequence as the "secondary site" and, taken together,

make up the extended DNA recognition element recognized by LiaR family members (Figure 5a). In this case the extended protected sequence over a site size of 45 base pairs suggests binding of two dimers or a single tetramer.

For the *liaFS*R promoter only about 29 (−77 to −48) nucleotides are protected (Figure 5c). The size of the DNase footprint is comparable to that observed for the *Efc liaFSR* operon. As we observed for the *Efc liaFSR* operon, in addition to the predicted consensus site (−77 to −62), there is a distinct protection for a secondary site from −63 to −48. Since the protected region for *Efm liaFSR* is smaller (29 base pairs) than that of *Efm liaXYZ* (45 base pairs) the evidence for two dimers of LiaR binding to the *Efm liaFSR* operon is less clear. In the comparable *Efc liaFSR* operon, the inclusion of the extended region was necessary for high affinity [19]. It is also interesting to note that the organization of the *liaFSR* and *liaXYZ* operons is very different. For *liaXYZ* the secondary site is 5' of the consensus site while in *liaFSR* the secondary site is 3' of the consensus sequence (Figure 5). This organization was also observed in *E. faecalis*.

While the protection sites of LiaR in *E. faecium* for both operons are identical in size for the closely related species, *E. faecalis* [19], the recognition elements for the *E. faecium liaFSR* and *liaXYZ* operons are shifted 4 and 16 base pairs respectively closer to the translation start site.

DNase hypersensitive sites suggest long range changes to DNA structure upon LiaR binding

In addition to protection from DNase cleavage, protein binding can also induce changes in DNA structure that increase nuclease sensitivity (hypersensitivity). Hypersensitivity is often correlated with bending or kinks induced in the DNA structure that render the phosphodiester backbone more accessible. As shown in Figure 5, both consensus binding regions share a strong hypersensitive site at the T immediately 3' of the A in the consensus sequence ($T(X)_4C(X)_4G(X)_4\underline{\mathbf{A}}$) a feature also observed in the homologous *E. faecalis* sequences.

Additional evidence for long range DNA structural changes suggestive of DNA bending can be seen as subtle hypersensitive sites at positions −85 and −53 of the *liaFSR* operon. As in the *Efm liaFSR* protection pattern, the protected region within *liaXYZ* operon is flanked by two strong hypersensitive sites at −79 and −114. These additional hypersensitive sites (−85 and −53 within *liaFSR* operon and −114 within *liaXYZ* operon) were not observed previously in the *E. faecalis* species. In *E. faecalis*, we had previously identified a region of marked hypersensitivity to nuclease digestion located 35 bases downstream of the *liaXYZ* consensus sequence [19]. Although this specific hypersensitive site was not present in *E. faecium* there is a strong and consistent hypersensitive site at positions (−4) AGCG (−1) (Figure 5e) of *Efm liaFSR*. Thus, our findings suggest that LiaR can significantly change the structure of DNA up to 50 bp downstream of the binding site, which could modify transcription rates.

The adaptive mutant *Efm* LiaR^{W73C} binds more tightly to DNA binding sites within the *liaXYZ* and *liaFSR* operons

We have reported previously that the adaptive mutant LiaR^{D191N} that is associated with daptomycin resistance in *E. faecalis* S613, markedly increases LiaR affinity for target DNA sequences and thereby upregulates transcription of LiaR-controlled genes [19]. Here, we tested the hypothesis that *Efm* LiaR^{W73C} may have a similar effect on binding to specific DNA sequences. Using MicroScale Thermophoresis (MST), we measured the affinity of LiaR for both the consensus and adjoining secondary sites separately as well as for the entire protection region that were recovered from our DNA footprint analysis (Figure 6). We found that *Efm* LiaR^{W73C} has an increased affinity for DNA target sites compared to wild-type LiaR to both the consensus and secondary sequences of the *liaXYZ* operon, consistent with our earlier observation of increased affinity for DNA by the adaptive mutant *Efc* LiaR^{D191N} (Table 2, Figure 6a). However, the affinities of full-length *Efm* LiaR^{W73C} toward cognate DNA measured in this study are generally weaker than those reported for *Efc* LiaR^{D191N}. Unlike *Efc* LiaR^{D191N}, which had higher affinity for the consensus site (0.39 ± 0.03 μM), *Efm* LiaR^{W73C} binds with comparable affinity to both the consensus and secondary sites (9.9±0.6 μM and 16.7±0.4 μM, respectively).

We would have also expected *Efm* LiaR^{W73C} to bind with higher affinity to the entire contiguous protected region identified by DNA footprinting for the *liaXYZ* operon. However, the binding affinity was comparable to that for the consensus site alone (*liaXYZ*: Kd = 13.7±1.3 versus 9.9±0.6 μM) (Table 2). Interestingly, the binding isotherms for the entire protected region indicate a clear positive cooperativity in binding as well. It is not clear whether the apparent cooperativity results from direct dimer-dimer interactions of LiaR dimers at the DNA or from a strong shift of the LiaR monomer-dimer equilibrium in the presence of DNA. We favor the latter as the apparent cooperativity could be observed on the smaller 26 nucleotide DNA substrates that would not accommodate two dimers.

While DNA protection studies revealed that *Efm* LiaR had regions of protection that extended well beyond the consensus binding sequence, the overall affinity for the *liaFSR* and *liaXYZ* consensus sequences was quite different. The affinity of LiaR^{W73C} for a 26 nucleotide DNA sequence extending from −83 to −58 (Figure 5c, d) of *liaFSR* was at least 10–fold lower than the comparable *liaXYZ* consensus binding site (Table 2). To test whether the additional sequences protected outside the canonical *liaFSR* consensus binding site are important for *Efm* LiaR binding, we extended the DNA sequence an additional 6 nucleotides toward the translation start site and measured the affinity for this extended 32 nucleotides protected region by MST. *Efm* LiaR^{W73C} binds to the extended sequence at a micromolar concentration K_d=18.2±1.1 μM or about 5-fold higher than the shorter consensus site alone. The affinity for the entire contiguous protected region for *Efm liaFSR* (46 nucleotides, see Figure 5d) was comparable to that for the extended site K_d=13.3±1.3 μM (Table2). This is consistent with our earlier findings for *Efc* LiaR binding to the *Efc liaFSR* operon and confirming our earlier hypothesis that DNA sequences adjoining the canonical consensus sequence of the *Efm liaFSR* operon are also important for DNA binding.

The DNA binding domain alone is not able to bind regulatory DNA sequences with high affinity

Our analytical ultracentrifugation studies had demonstrated that the *Efm* LiaR^{DBD} were able to dimerize readily in solution implying that it might have been possible for the DNA binding domains alone to have high affinity for DNA. The binding of *Efm* LiaR^{DBD} to the *liaXYZ* and *liaFSR* operon sequences did not generate enough fluorescence change to obtain reliable K_d suggesting extremely weak protein–DNA interactions. These results support our earlier observation that even though the DNA binding domain itself exists in solution as a dimer, with a K_d of 0.4 μM (Table 1), the receiver domain appears essential for specific DNA binding.

Discussion

Exploration of the membrane stress response pathways of the pathogens *E. faecium, E. faecalis* and *S. aureus* reveals many commonalities as well as significant differences that should frame discussions of new therapies and antimicrobials. Examination of LiaR from *E. faecium* and *E. faecalis* and its homolog from *S. aureus,* VraR suggests an interesting evolutionary flexibility in the response regulator quaternary structure. *E. faecium* LiaR and *S. aureus* VraR are largely monomeric and become dimeric upon phosphorylation to mediate the cell membrane stress response. In contrast, *E. faecalis* LiaR exists predominately as a dimer that oligomerizes to an active tetramer upon phosphorylation [19]. DNA footprinting analysis of upstream regulatory regions from all three organisms suggests extended footprints that extend beyond the simple predicted consensus sequence upon phosphorylation or activation by an adaptive substitution. In principle, such extended DNA binding regions could be bound as a pair of dimers or as a single tetramer in the case of *Efc* LiaR. In the crystal structures of both *S. aureus* VraR and *Efm* LiaR there are two pairs of dimers in the asymmetric unit that could reflect how they might bind to extended regions of DNA and produce DNA bending to facilitate recruitment of RNA polymerase. Indeed our DNA footprinting studies for both *Efc* and *Efm* LiaR suggest that LiaR binding induces strong DNase hypersensitive sites suggestive of DNA bending. If DNA recognition by this family of response regulators requires four copies of the protein to induce DNA bending and a consequent increase in transcription from target operons, then any mutation that favors oligomerization will effectively “turn on” the system. This has now been observed in the adaptive mutants *Efc* LiaR^{D191N} and *Efm* LiaR^{W73C} isolated in response to the antimicrobial peptide daptomycin.

Interestingly, the activating substitution in *Efc* LiaR occurs at position 73 of the receiver domain and is not at the dimerization surface of the receiver domain dimer. (Figure 7a). The fact that the adaptive mutation W73→C in *Efm* LiaR is distant from the molecular interfaces comprising a LiaR dimer suggests an indirect role in favoring the dimerization competent monomer (e.g., the phosphorylated state). Based on our SEQ results in the absence of BeF_3^-, the full length LiaR protein is monomeric. In contrast, the sedimentation equilibrium analysis showed a weak but detectable dimerization propensity (K_d = 676 μM) for the LiaR receiver domain (LiaRRD) and a much stronger propensity for the DNA binding domain (LiaR^{DBD}) to dimerize (K_d = 0.4 μM). Based on these results, we suggest a model where the

receiver domain and DNA binding domain interact with each other in the unphosphorylated LiaR protein, stabilizing the monomeric state of the protein and preventing dimerization of either the receiver domains or the DNA binding domain ("closed" state). However, phosphorylation dependent conformational changes or the substitution W73C in the receiver domain may promote the dissociation of the receiver domain from the DNA binding domain, allowing dimerization of both the receiver domain and the DNA binding domains of two LiaR protomers. A closed state has been observed previously in crystal structures of the unphosphorylated VraR and NarL proteins [28, 36]. In these reported structures, the dimerization surface of the DNA binding domain helix α-10 of VraR or helix α-9 of NarL were found to be buried against the receiver domain of the respective protomer to stabilize a closed monomer conformation. Although the exact amino acids involved in this interdomain interface are not conserved across the NarL/FixJ family of response regulators, the general paradigm has been observed in other family members [27].

In the absence of a structure for the full length unphosphorylated wild type *E. faecium* LiaR, we mapped the *Efm* LiaR^{W73C} onto the VraR (PDB ID 4GVP)/NarL (PDB ID 1RNL) structures. As shown in Figure 7b, if our unphosphorylated LiaR structure resembles the inactive NarL but not VraR structure, the Trp73 is in the interfacial contact surface of the receiver to DNA binding domain. Thus the molecular surface comprised in part by Trp73 may be important for stabilizing the closed monomer conformation where the receiver domain interacts with the DNA binding domain of the same protomer chain. The W73C substitution may weaken the interface between the receiver domain and the DNA binding domain, shifting the equilibrium from the closed state to an open state where the receiver and DNA binding domains have a higher propensity to dimerize with another LiaR monomer to form the activated dimer. Alternatively, we cannot rule out the possibility that the molecular dynamics of the receiver domain is altered in a more indirect manner to shift the LiaR ensemble towards a state that more closely resembles the phosphorylated state.

There are at least two biological contexts where increased dimerization can lead to upregulation of the LiaR regulon. The most obvious scenario is one in which LiaR^{W73C} increases phosphorylation independent dimerization to constitutively hyperactivate the LiaFSR stress response pathway. This LiaS independent constitutive hyperactivation mechanism was observed for the *Efc* LiaR^{D191N} adaptive mutant [19]. It is puzzling however that *Efm* LiaR^{W73C} does not actually confer the same extent of dimerization as BeF_3^- stimulated wild type *Efm* LiaR (wild type *Efm* LiaR dimerization K_d was 15 μM compared to 236 μM for *Efm* LiaR^{W73C}). Since *in vivo* concentrations of LiaR are estimated to be in the low micromolar range [37], the weak *in vitro* dimerization of *Efm* LiaR^{W73C} is less than expected for constitutive hyperactivation. Alternatively, the *Efm* LiaR^{W73C} mutant may interact more efficiently with its cognate kinase LiaS to produce a higher extent of phosphorylation than the comparable wild type LiaR interaction with LiaS. This alternative possibility is made more attractive by the observation that the *Efm* LiaR^{W73C} mutation has always been identified with a LiaS^{T120A} in clinical daptomycin non-susceptible isolates [17]. In the case of *Efc* LiaR^{D191N}, a concomitant second mutation in the *Efc* LiaS protein has not been observed. Thus, there may be at least two distinct classes of adaptive mutations through changes in LiaR, a constitutive phosphorylation-independent hyperactivation type (as seen for *Efc* LiaR^{D191N}) and a second type that promotes more efficient phosphorylation

by LiaS that might include *Efm* LiaR^{W73C} and that may be frequently observed in epistatic combination with sunbstitutions in LiaS.

If adaptive LiaR substitutions that favor oligomerization confer additional resistance to membrane stress, then, it is also likely that any small molecule that destabilizes oligomerization will increase susceptibility. Support for this hypothesis is observed readily in a recently described *Efc* [16] *liaR* knockout. When *Efc liaR* is removed, cells become hypersusceptible to daptomycin suggesting that LiaR could be a good target for new drugs that would complement existing antibiotics to maintain their long term efficacy by blocking the evolution of resistance through *liaR* [16].

Evolutionarily, there appears to be a spectrum of oligomeric answers to the question of how to bind these specific and extended DNA sequences. We have now observed both a monomer↔dimer and a dimer↔tetramer transition upon phosphorylation depending on the species. In all cases however, the DNA regulatory region is extended. Some organisms like *S. aureus* and *E. faecium* may shift the equilibrium towards the monomer while others like *E. faecalis* start as a dimer (that presumably does not bind DNA with high enough affinity to activate as a dimer alone) and then activate transcription as a tetramer. The facile nature of these equilibrium shifts can be seen readily by the single point mutations that dramatically change the oligomeric state (e.g. LiaR^{D191N} and LiaR^{W73C} in *E. faecalis* and *E. faecium*, respectively) (Figure 8)

More recently, a new *Efm* LiaR mutant *Efm* LiaR^{S19F} has been identified in DAP non-susceptible enterococci isolated from an immunocompromised patient suggesting that mutations within the receiver domain may be more common in *E. faecium* [38]. Mapping the recently discovered S19F substitution in the response regulator *Efm* LiaR onto our LiaR three-dimensional crystal structure (Figure 7a) revealed that this mutation is within the receiver domain dimerization interface. Based on our studies, the *Efm* LiaR S19F substitution may also increase oligomerization of LiaR to form a constitutively activated dimer with high affinity for the extended DNA regulatory sequence even in the absence of phosphorylation, leading to increased daptomycin resistance. If single point mutations can produce such large changes then it is not surprising that evolution has tuned these systems in particular niches. What might be surprising is that *E. faecium* would be so different from *E. faecalis* but perhaps this is the bias introduced by nomenclature rather than biology. *E. faecium* (GenBank accession number: **WP_002348688.1**) is 60.5 % identical to *S. aureus* (GenBank accession number: **WP_000153535.1**) while *E. faecalis* (GenBank accession number: **EFE19096.1**) is 59.7 % identical to *S. aureus. E. faecalis* and *E. faecium* themselves share 84.3% identity and thus there is substantial genomic variability to allow for these surprising differences (Figure S7). For example, *E. faecalis* LiaR has a deletion within the N-terminal ß1 strand (Figure S7) that is not present in *E. faecium* LiaR or *S. aureus* VraR. The truncation at the N-terminus is unusual within the NarL/FixJ subfamily and further highlights that even among closely related species there may be variability within protein structure with important consequences for protein function.

Interestingly *E. faecium* in the initial stages (only when the LiaFSR mutation occurs) is able to carry out both diversion and repulsion strategies while *S. aureus* favors repulsion and *E.*

faecalis favors diversion. These distinctive phenotypic changes suggest *E. faecium* may have some quite unique responses to membrane stress that contrasts markedly with its closely related peers.

Experimental procedures

Expression and purification of response regulator R494 LiaR and variants from *E. faecium*

The genes encoding full length LiaR^{W73C} R494, receiver domain (RD^{W73C}, residues 1-139) and DNA binding domain (DBD, residues 140-210) were amplified by PCR from genomic DNA R494, cloned into pETDuet vector and expressed in *Escherichia coli* BL21 (DE3) cells using LB medium. Site-directed mutagenesis of LiaR was performed by incorporation of mutations into the plasmid by inverse PCR with standard primers designed an overlapping orientation. The proteins were purified with a nickel affinity column (GE Healthcare) followed by the anion-exchange chromatography and gel filtration for the final step as described previously work [19]. N-terminal SUMO peptide (within the 6×His tag) was removed by treatment with His-tagged SUMO protease.

DNA footprint analysis by automated capillary electrophoresis (DFACE)

The 379-bp fluorescent labeled DNA probe for the R494 *E. faecium liaFSR* operon and 357-bp fluorescent labeled DNA probe for the R494 *E. faecium liaXYZ* operon were generated with PCR amplification with the primers 5'-(VIC)-aatgattctcctatcgcgcaagca-3' and 5'-(FAM)-actaaaagcaaaaatccagtattg-3' for *liaFSR* operon and 5'-(VIC)-agcgttgatcctctggtttattga-3' and 5'-(FAM)-aagccttcttcagtcgaaaggatt-3' *liaXYZ* operon from Applied Biosystems (Grand Island, NY) as described previously [19, 39, 40]. Briefly, full length of *Efm* LiaR protein activated with the BeF_3^- at 0.5, 2.5, 5 μM and 50.0 μM was then incubated with respective fluorescent labeled DNA probe in Binding Buffer (50 mM Tris pH 7.5, 300 mM NaCl, 10 mM $MgCl_2$, and 0.3 mM DTT, 20% (v/v) glycerol, 0.05% (v/v) Tween-20) for 10 min. After this incubation, DNase I (New England Biolabs Inc., Ipswich, MA, 2 U/μl) digestion was performed. The reaction was then stopped by adding EDTA to a final concentration of 5 mM following by incubation at 75°C for 10 min. Control digestions with the probe were performed in the absence of the protein. The DNA fragments were purified with a QIA-quick PCR purification kit (Qiagen, Valencia, CA) and then sent to the Plant-Microbe Genomics Facility for further analysis. The resulting electropherograms from the DFACE assay were analyzed with the software GeneMapper 4.0 set to normalize all samples to the sum of the signal of all samples. In addition, the histograms were further normalized by subtracting the height of the equivalent peak (same Bin) in the negative control from the sample, i.e. each bar is the difference between sample and negative control. Data reported utilized fragments/strand labeled with VIC dye. Nucleotide positions refer to the region of LiaR binding on the DNA relative to the translation start site of LiaX or LiaF, respectively. DNA footprinting was performed at 25°C.

Analytical Ultracentrifugation

Sedimentation equilibrium analytical ultracentrifugation (SEQ) and sedimentation velocity) experiments were performed in an AnTi60 rotor or AnTi50 rotor respectively, at 20°C using a Beckman XL-I instrument. Epon double sector centerpieces and sapphire windows. The

protein samples were prepared in either 50 mM Tris-HCl, 300 mM NaCl, 10 mM $MgCl_2$, 2 mM Tris(2-carboxyethyl)phosphine and 10% (v/v) glycerol at pH 7.5 or 50 mM Tris-HCl, 300 mM NaCl, 10 mM $MgCl_2$, 2 mM tris(2-carboxyethyl)phosphine, 10% (v/v) glycerol, 5 mM $BeCl_2$ and 30 mM NaF at pH 7.5 to test the self-association of the protein(s) in the absence and presence of the phosphorylation mimetic Beryllofluoride (BeF_3^-) respectively. SEQ scans were using absorbance at 280 nm, after 64 h incubation at each rotor speed. The protein partial specific volume, solvent density and solvent viscosity were calculated using Sednterp 1.09 (1). SEQ scans were collected using absorbance at 280 nm, after 64 h incubation at each rotor speed. Sedimentation equilibrium analytical ultracentrifugation analysis for *Efm* LiaR, LiaR:BeF_3^-, $LiaR^{W73C}$, $LiaR^{W73C}$:BeF_3^-, $LiaR^{RD}$, $LiaR^{RD}$:BeF_3^-, $LiaR^{(RD)W73C}$, $LiaR^{(RD)W73C}$:BeF_3^-, $LiaR^{DBD}$ recorded at 13000 r.p.m., 20000 r.p.m. and 25000 r.p.m. Data analysis was performed using Sedphat v10.58d (2,3). For each protein, the SEQ profiles were globally fitted to a monomer-dimer equilibrium model with rotor stretch and mass conservation restraints. A F-statistics error mapping approach was used to determine the 95% confidence intervals for the dissociation constant [41-44]. Sedimentation velocity (SV) data, recorded at 50000 r.p.m., was fitted using a local continuous distribution model looking for species between 0.5 and 15 Svedbergs with the frictional ratio, meniscus and bottom position allow to float to find the best fit. A single discrete species was included in the model with a sedimentation coefficient of 0.3 Svedbergs, to account for any buffer component effects. The Tikhonov regularization for the c(S) and c(M) distributions was set to 0.95.

DNA binding affinity determination by Microscale Thermophoresis (MST)

MST measurements were done as described previously [19, 45]. Briefly, a solution of unlabeled LiaR (wild type or mutants) was serially diluted in reaction buffer (50 mM Tris pH 7.5, 300 mM NaCl, 10 mM $MgCl_2$, 0.3 mM DTT, 10% glycerol, 0.05% (v/v) Tween-20) to which an equal volume of Alexa-647 labeled DNA was added to a final concentration of 40 nM. The samples were loaded into standard treated capillaries (Nanotemper). MST experiments were measured on a Monolith NT.115 system (Nanotemper Technologies) using 30% LED and 90% IR-laser power. The resulting K_d values based on average from four independent MST measurements. Temperature of MST experiments was 20°C. Data analyses were performed using Nanotemper Analysis software, v.1.5.41. (Supplementary information).

Structure determination of full length LiaR activated by BeF_3^-

A beryllofluoride activated LiaR protein crystal suitable for data collection was grown at 10° C in 0.1 M magnesium formate dehydrate, 15 % w/v Polyethylene glycol 3,350 using a ‘microseed matrix screening’ approach [46]. Diffraction data were collected at Argonne National Laboratory’s Advanced Photon Source (ANL APS) beamline 21-ID-D on a MarMosaic 300 CCD detector. X-ray diffraction data were processed using HKL2000 [47]. The crystal belonged to the space group $P3_1$ with the unit cell parameters a=31.05, b=76.92, c=76.92, $\alpha=\beta=\gamma=90°$. The 3-D structure was determined by molecular replacement using *S. aureus* receiver and DNA binding domains as the search probe in Phaser-MR [48].The solution from molecular replacement suggested four molecules in the asymmetric unit and a Matthews coefficient of 3.03 (59.5% solvent content) [49].

The structure was refined to 3.2 Å resolution using the Phenix suite [50] and Coot [51]. The final values for the R=21.86 % and R_{free} factors are 27.04 %. A summary of data collection and refinement statistic are reported in Table 3.

Supplementary Material

Refer to Web version on PubMed Central for supplementary material.

Acknowledgements

This work was supported by National Institutes of Health Grant [R01AI080714 to Y.S.]; [R21AI1114961-01 to C.A.]; [R21/331R21AI121519-01 to C.A.]. The Rice University Crystallographic Core Facility is supported by a Kresge Science Initiative endowment grant. We would like to thank the staff at ANL APS for their support during the data collection.

Abbreviations used

VRE	Vancomycin-resistant enterococci
HAI	Hospital-Associated Infections
IDSA	Infectious Diseases Society of America
SEQ	sedimentation equilibrium analytical ultracentrifugation
MST	MicroScale Thermophoresis
DFACE	DNA footprint analysis by automated capillary electrophoresis

References

[1]. Arias CA, Murray BE. The rise of the Enterococcus: beyond vancomycin resistance. Nat Rev Microbiol. 2012; 10:266–78. [PubMed: 22421879]

[2]. Boucher HW, Talbot GH, Bradley JS, Edwards JE, Gilbert D, Rice LB, et al. Bad bugs, no drugs: no ESKAPE! An update from the Infectious Diseases Society of America. Clin Infect Dis. 2009; 48:1–12. [PubMed: 19035777]

[3]. Munita JM, Murray BE, Arias CA. Daptomycin for the treatment of bacteraemia due to vancomycin-resistant enterococci. Int J Antimicrob Agents. 2014; 44:387–95. [PubMed: 25261158]

[4]. Fowler VG Jr. Boucher HW, Corey GR, Abrutyn E, Karchmer AW, Rupp ME, et al. Daptomycin versus standard therapy for bacteremia and endocarditis caused by Staphylococcus aureus. N Engl J Med. 2006; 355:653–65. [PubMed: 16914701]

[5]. Humphries RM, Pollett S, Sakoulas G. A current perspective on daptomycin for the clinical microbiologist. Clin Microbiol Rev. 2013; 26:759–80. [PubMed: 24092854]

[6]. Tran TT, Panesso D, Mishra NN, Mileykovskaya E, Guan Z, Munita JM, et al. Daptomycin-resistant Enterococcus faecalis diverts the antibiotic molecule from the division septum and remodels cell membrane phospholipids. MBio. 2013; 4:e00281–13. [PubMed: 23882013]

[7]. Pogliano J, Pogliano N, Silverman JA. Daptomycin-mediated reorganization of membrane architecture causes mislocalization of essential cell division proteins. J Bacteriol. 2012; 194:4494–504. [PubMed: 22661688]

[8]. Cha R, Rybak MJ. Influence of protein binding under controlled conditions on the bactericidal activity of daptomycin in an in vitro pharmacodynamic model. J Antimicrob Chemother. 2004; 54:259–62. [PubMed: 15150172]

[9]. Fuchs PC, Barry AL, Brown SD. In vitro bactericidal activity of daptomycin against staphylococci. J Antimicrob Chemother. 2002; 49:467–70. [PubMed: 11864946]

[10]. Cotroneo N, Harris R, Perlmutter N, Beveridge T, Silverman JA. Daptomycin exerts bactericidal activity without lysis of Staphylococcus aureus. Antimicrob Agents Chemother. 2008; 52:2223–5. [PubMed: 18378708]

[11]. Silverman JA, Perlmutter NG, Shapiro HM. Correlation of daptomycin bactericidal activity and membrane depolarization in Staphylococcus aureus. Antimicrob Agents Chemother. 2003; 47:2538–44. [PubMed: 12878516]

[12]. Jung D, Rozek A, Okon M, Hancock RE. Structural transitions as determinants of the action of the calcium-dependent antibiotic daptomycin. Chem Biol. 2004; 11:949–57. [PubMed: 15271353]

[13]. Tran TT, Munita JM, Arias CA. Mechanisms of drug resistance: daptomycin resistance. Ann N Y Acad Sci. 2015; 1354:32–53. [PubMed: 26495887]

[14]. Hachmann AB, Angert ER, Helmann JD. Genetic analysis of factors affecting susceptibility of Bacillus subtilis to daptomycin. Antimicrob Agents Chemother. 2009; 53:1598–609. [PubMed: 19164152]

[15]. Hachmann AB, Sevim E, Gaballa A, Popham DL, Antelmann H, Helmann JD. Reduction in membrane phosphatidylglycerol content leads to daptomycin resistance in Bacillus subtilis. Antimicrob Agents Chemother. 2011; 55:4326–37. [PubMed: 21709092]

[16]. Reyes J, Panesso D, Tran TT, Mishra NN, Cruz MR, Munita JM, et al. A liaR Deletion Restores Susceptibility to Daptomycin and Antimicrobial Peptides in Multidrug-Resistant Enterococcus faecalis. J Infect Dis. 2014

[17]. Diaz L, Tran TT, Munita JM, Miller WR, Rincon S, Carvajal LP, et al. Whole-genome analyses of Enterococcus faecium isolates with diverse daptomycin MICs. Antimicrob Agents Chemother. 2014; 58:4527–34. [PubMed: 24867964]

[18]. Miller C, Kong J, Tran TT, Arias CA, Saxer G, Shamoo Y. Adaptation of Enterococcus faecalis to daptomycin reveals an ordered progression to resistance. Antimicrob Agents Chemother. 2013; 57:5373–83. [PubMed: 23959318]

[19]. Davlieva M, Shi Y, Leonard PG, Johnson TA, Zianni MR, Arias CA, et al. A variable DNA recognition site organization establishes the LiaR-mediated cell envelope stress response of enterococci to daptomycin. Nucleic Acids Res. 2015; 43:4758–73. [PubMed: 25897118]

[20]. Belcheva A, Golemi-Kotra D. A close-up view of the VraSR two-component system. A mediator of Staphylococcus aureus response to cell wall damage. J Biol Chem. 2008; 283:12354–64. [PubMed: 18326495]

[21]. Cho H, Wang W, Kim R, Yokota H, Damo S, Kim SH, et al. BeF(3)(−) acts as a phosphate analog in proteins phosphorylated on aspartate: structure of a BeF(3)(−) complex with phosphoserine phosphatase. Proc Natl Acad Sci U S A. 2001; 98:8525–30. [PubMed: 11438683]

[22]. Varughese KI, Tsigelny I, Zhao H. The crystal structure of beryllofluoride Spo0F in complex with the phosphotransferase Spo0B represents a phosphotransfer pretransition state. J Bacteriol. 2006; 188:4970–7. [PubMed: 16788205]

[23]. Munita JM, Panesso D, Diaz L, Tran TT, Reyes J, Wanger A, et al. Correlation between mutations in liaFSR of Enterococcus faecium and MIC of daptomycin: revisiting daptomycin breakpoints. Antimicrob Agents Chemother. 2012; 56:4354–9. [PubMed: 22664970]

[24]. Galperin MY. Structural classification of bacterial response regulators: diversity of output domains and domain combinations. J Bacteriol. 2006; 188:4169–82. [PubMed: 16740923]

[25]. Robinson VL, Buckler DR, Stock AM. A tale of two components: a novel kinase and a regulatory switch. Nat Struct Biol. 2000; 7:626–33. [PubMed: 10932244]

[26]. Thomas SA, Brewster JA, Bourret RB. Two variable active site residues modulate response regulator phosphoryl group stability. Mol Microbiol. 2008; 69:453–65. [PubMed: 18557815]

[27]. Trajtenberg F, Albanesi D, Ruetalo N, Botti H, Mechaly AE, Nieves M, et al. Allosteric activation of bacterial response regulators: the role of the cognate histidine kinase beyond phosphorylation. MBio. 2014; 5:e02105. [PubMed: 25406381]

[28]. Leonard PG, Golemi-Kotra D, Stock AM. Phosphorylation-dependent conformational changes and domain rearrangements in Staphylococcus aureus VraR activation. Proc Natl Acad Sci U S A. 2013; 110:8525–30. [PubMed: 23650349]

[29]. Mack TR, Gao R, Stock AM. Probing the roles of the two different dimers mediated by the receiver domain of the response regulator PhoB. J Mol Biol. 2009; 389:349–64. [PubMed: 19371748]

[30]. Barbieri CM, Wu T, Stock AM. Comprehensive analysis of OmpR phosphorylation, dimerization, and DNA binding supports a canonical model for activation. J Mol Biol. 2013; 425:1612–26. [PubMed: 23399542]

[31]. Birck C, Mourey L, Gouet P, Fabry B, Schumacher J, Rousseau P, et al. Conformational changes induced by phosphorylation of the FixJ receiver domain. Structure. 1999; 7:1505–15. [PubMed: 10647181]

[32]. Baikalov I, Schroder I, Kaczor-Grzeskowiak M, Cascio D, Gunsalus RP, Dickerson RE. NarL dimerization? Suggestive evidence from a new crystal form. Biochemistry. 1998; 37:3665–76. [PubMed: 9521685]

[33]. Schnell R, Ågren D, Schneider G. 1.9 Å structure of the signal receiver domain of the putative response regulator NarL from Mycobacterium tuberculosis. Acta Crystallogr Sect F Struct Biol Cryst Commun. 2008; 64:1096–100.

[34]. Webber CA, Kadner RJ. Involvement of the amino-terminal phosphorylation module of UhpA in activation of uhpT transcription in Escherichia coli. Mol Microbiol. 1997; 24:1039–48. [PubMed: 9220010]

[35]. Maiti R, Van Domselaar GH, Zhang H, Wishart DS. SuperPose: a simple server for sophisticated structural superposition. Nucleic Acids Res. 2004; 32:W590–4. [PubMed: 15215457]

[36]. Baikalov I, Schroder I, Kaczor-Grzeskowiak M, Grzeskowiak K, Gunsalus RP, Dickerson RE. Structure of the Escherichia coli response regulator NarL. Biochemistry. 1996; 35:11053–61. [PubMed: 8780507]

[37]. Belcheva A, Verma V, Korenevsky A, Fridman M, Kumar K, Golemi-Kotra D. Roles of DNA sequence and sigma A factor in transcription of the vraSR operon. J Bacteriol. 2012; 194:61–71. [PubMed: 22020638]

[38]. Sorlozano A, Panesso D, Navarro-Mari JM, Arias CA, Gutierrez-Fernandez J. Characterization of daptomycin non-susceptible Enterococcus faecium producing urinary tract infection in a renal transplant recipient. Rev Esp Quimioter. 2015; 28:207–9. [PubMed: 26200029]

[39]. Zianni M, Tessanne K, Merighi M, Laguna R, Tabita FR. Identification of the DNA bases of a DNase I footprint by the use of dye primer sequencing on an automated capillary DNA analysis instrument. J Biomol Tech. 2006; 17:103–13. [PubMed: 16741237]

[40]. Joshi GS, Zianni M, Bobst CE, Tabita FR. Further Unraveling the Regulatory Twist by Elucidating Metabolic Coinducer-Mediated CbbR-cbbI Promoter Interactions in Rhodopseudomonas palustris CGA010. J Bacteriol. 2012:1350–60. [PubMed: 22247506]

[41]. Laue, TM.; Shah, BD.; Ridgeway, TM.; Pelletier, SL. Computer-aided interpretation of analytical sedimentation data for proteins. Analytical Ultracentrifugation in Biochemistry and Polymer Science. In: S. E. Harding AJRaJCH. , editor. Royal Society of Chemistry; Cambridge: 1992.

[42]. Schuck P. On the analysis of protein self-association by sedimentation velocity analytical ultracentrifugation. Anal Biochem. 2003; 320:104–24. [PubMed: 12895474]

[43]. Vistica J, Dam J, Balbo A, Yikilmaz E, Mariuzza RA, Rouault TA, et al. Sedimentation equilibrium analysis of protein interactions with global implicit mass conservation constraints and systematic noise decomposition. Anal Biochem. 2004; 326:234–56. [PubMed: 15003564]

[44]. Johnson, ML.; Straume, M. Modern Analytical Ultracentrifugation. Birkhäuser; Boston: 1994. Comments on the analysis of sedimentation equilibrium experiments.

[45]. Jerabek-Willemsen M, Wienken CJ, Braun D, Baaske P, Duhr S. Molecular interaction studies using microscale thermophoresis. Assay Drug Dev Technol. 2011; 9:342–53. [PubMed: 21812660]

[46]. Obmolova G, Malia TJ, Teplyakov A, Sweet RW, Gilliland GL. Protein crystallization with microseed matrix screening: application to human germline antibody Fabs. Acta Crystallogr F Struct Biol Commun. 2014; 70:1107–15. [PubMed: 25084393]

[47]. Otwinowski, Z.; Minor, W. [20] Processing of X-ray diffraction data collected in oscillation mode. In: Carter, Charles W., Jr., editor. Methods in Enzymology. Academic Press; 1997. p. 307-26.

[48]. McCoy AJ, Grosse-Kunstleve RW, Adams PD, Winn MD, Storoni LC, Read RJ. Phaser crystallographic software. J Appl Crystallogr. 2007; 40:658–74. [PubMed: 19461840]

[49]. Kantardjieff KA, Rupp B. Matthews coefficient probabilities: Improved estimates for unit cell contents of proteins, DNA, and protein-nucleic acid complex crystals. Protein Sci. 2003; 12:1865–71. [PubMed: 12930986]

[50]. Adams PD, Afonine PV, Bunkoczi G, Chen VB, Davis IW, Echols N, et al. PHENIX: a comprehensive Python-based system for macromolecular structure solution. Acta Crystallogr D Biol Crystallogr. 2010; 66:213–21. [PubMed: 20124702]

[51]. Emsley P, Cowtan K. Coot: model-building tools for molecular graphics. Acta Crystallogr D Biol Crystallogr. 2004; 60:2126–32. [PubMed: 15572765]

Research Highlights

In clinical settings, nonsusceptibility to daptomycin by *Enterococcus faecium* is correlated frequently with a mutation in LiaR of Trp73 to Cys. To elucidate the physicochemical basis for LiaR mediated changes in daptomycin susceptibility, we used a combination of biophysical and structural approaches. Our study revealed that the adaptive mutation W73C, even in the absence of phosphorylation, activates LiaR to undergo a phosphorylation-like self-dimerization event that allows LiaR to recognize and activate upstream regulatory regions.

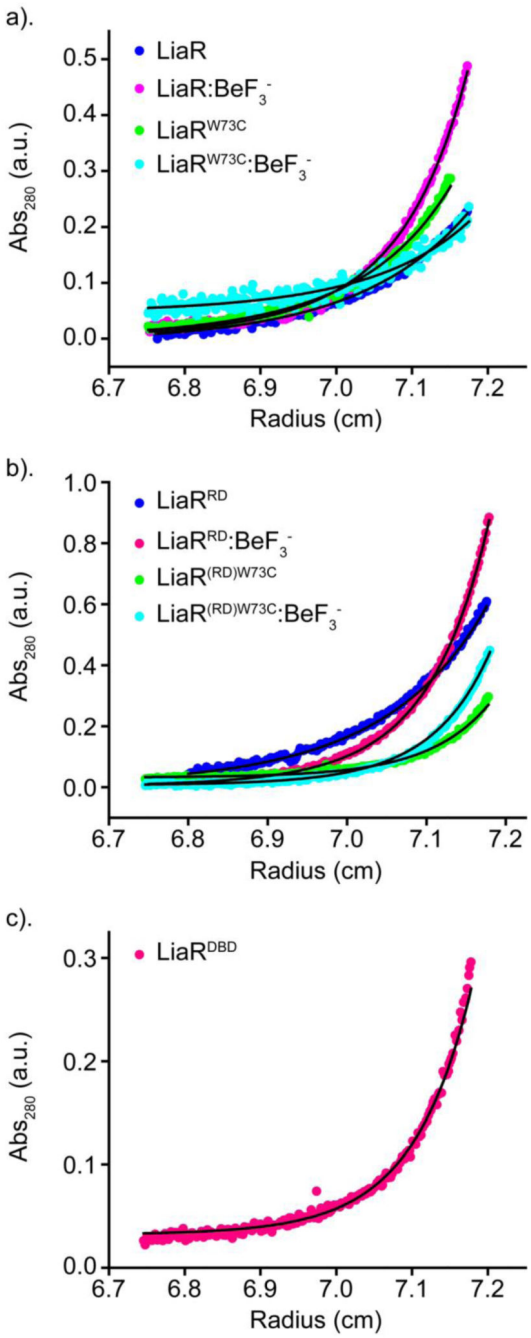

Figure 1. Beryllofluoride (BeF_3^-) promotes formation of *Efm* LiaR dimers

Sedimentation equilibrium analytical ultracentrifugation (AUC) profiles for: (a) full length *Efm* LiaR (dark blue); *Efm* LiaR with BeF_3^- (magenta); adaptive mutant *Efm* $LiaR^{W73C}$ (green); and adaptive mutant *Efm* $LiaR^{W73C}$ with BeF_3^- (cyan). (b) AUC profiles for *Efm* $LiaR^{(RD)}$ (blue); *Efm* $LiaR^{(RD)}$ with BeF_3^- (magenta); *Efm* $LiaR^{(RD)W73C}$ (green); and *Efm* $LiaR^{(RD)W73C}$ with BeF_3^- (cyan): (c) AUC profile for the DNA binding domain of *Efm* LiaR ($LiaR^{(DBD)}$) alone (magenta). For each protein, the SEQ profiles were globally fitted to a monomer only or monomer-dimer equilibrium model.

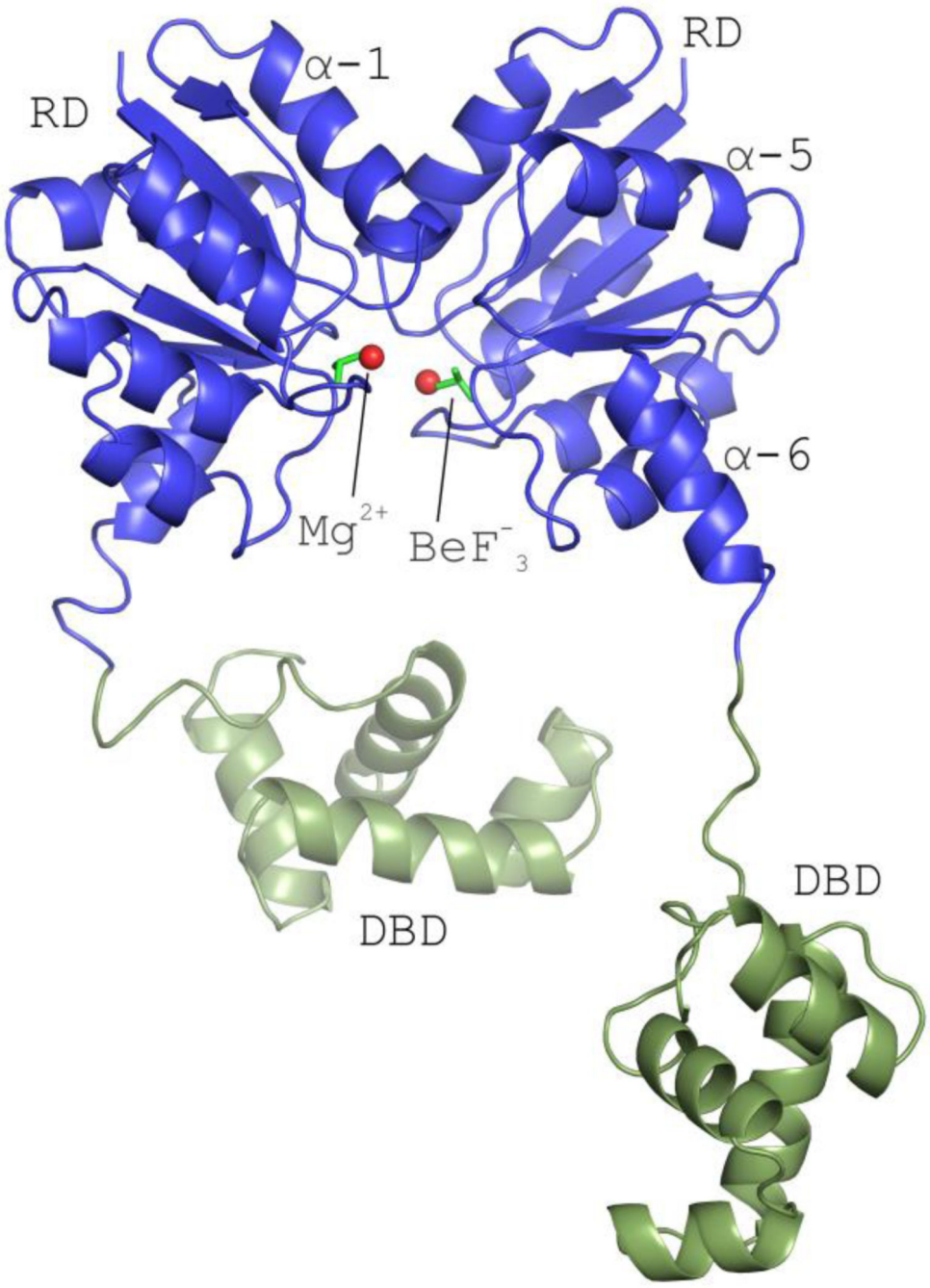

Figure 2. The structure of full-length *Efm* LiaR in complex with BeF_3^-/Mg^{2+} reveals an activated protein poised to bind DNA

Structural overview of the full length *Efm* LiaR activated with the BeF_3^- (PDB ID: **5HEV**). For clarity only one of the two pairs of LiaR dimers present in the asymmetric unit are displayed. Receiver domain (blue) showing a molecule of BeF_3^- bound proximal to the predicted phosphorylation site (Asp54). The LiaR dimerization surface is made up of the α-1 and α-5 helices. Mg^{2+} and BeF_3^- are shown as spheres (red) and sticks (dark green), respectively. Helix α-6 makes up part of the flexible linker joining the receiver and DNA-

binding domains (light green). The flexible linker allows the DNA binding domains to have a substantial amount of conformational flexibility to engage and bind to DNA.

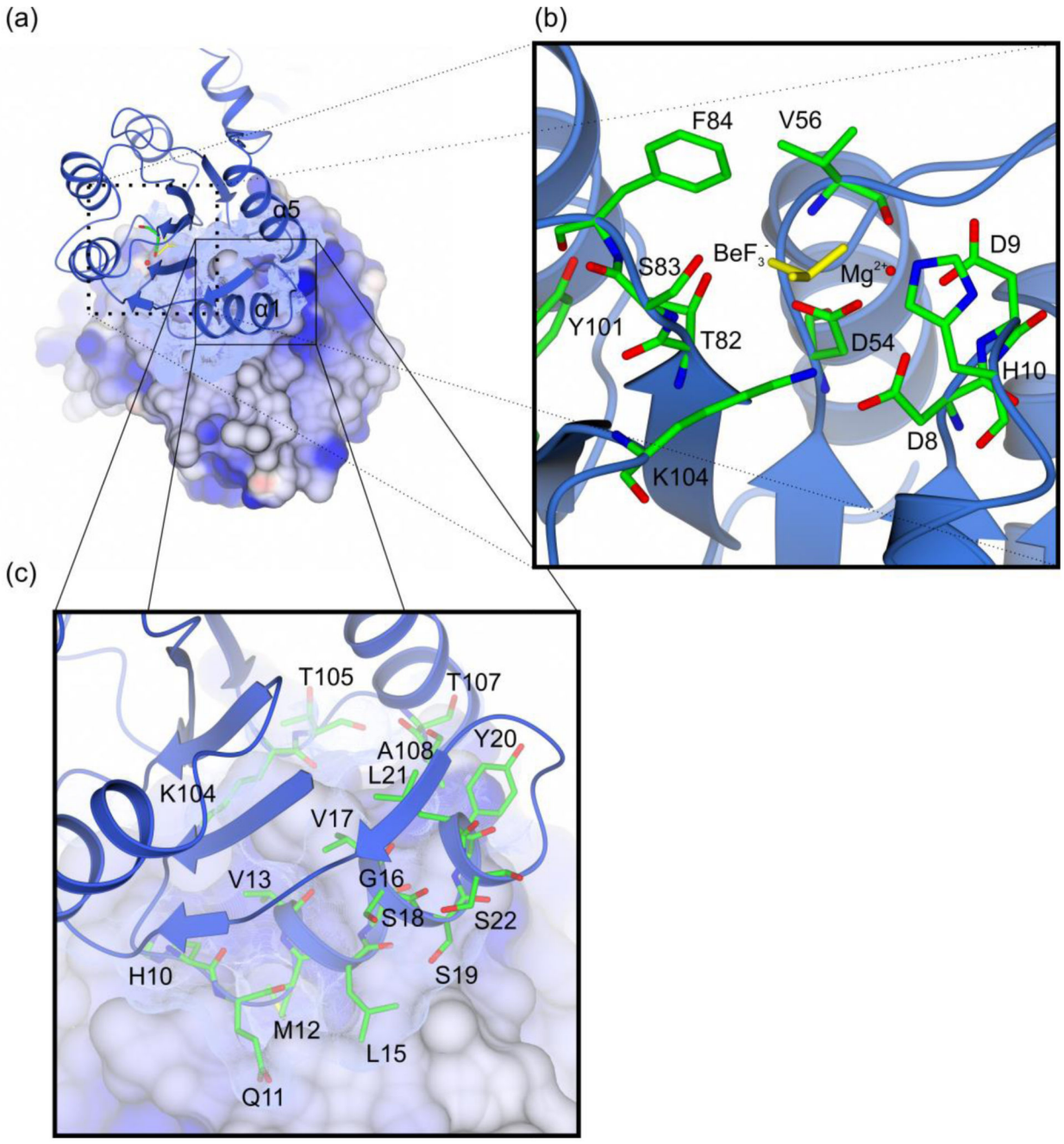

Figure 3. Overview of the LiaR receiver domain dimer

(a) The receiver domain forms a dimer through a hydrophobic interface of 692 Å^2 that juxtaposes the α1 and α5 helices of two LiaR protomers; (b) LiaR active site in the presence of BeF_3^- (yellow) and Mg^{2+} (red). The residues Thr83 and Tyr102, adopt a characteristic active conformation, toward the predicted phosphorylation site at Asp54. BeF_3^- is also in a position to make hydrogen bonds to Thr82 and Ser83 and a salt bridge to Lys104; (c) Key residues are shown that comprise the dimerization interface in a manner comparable to that

observed for VraR. Met12 from one protomer docks into a hydrophobic pocket within the dimerization interface of the second LiaR protomer.

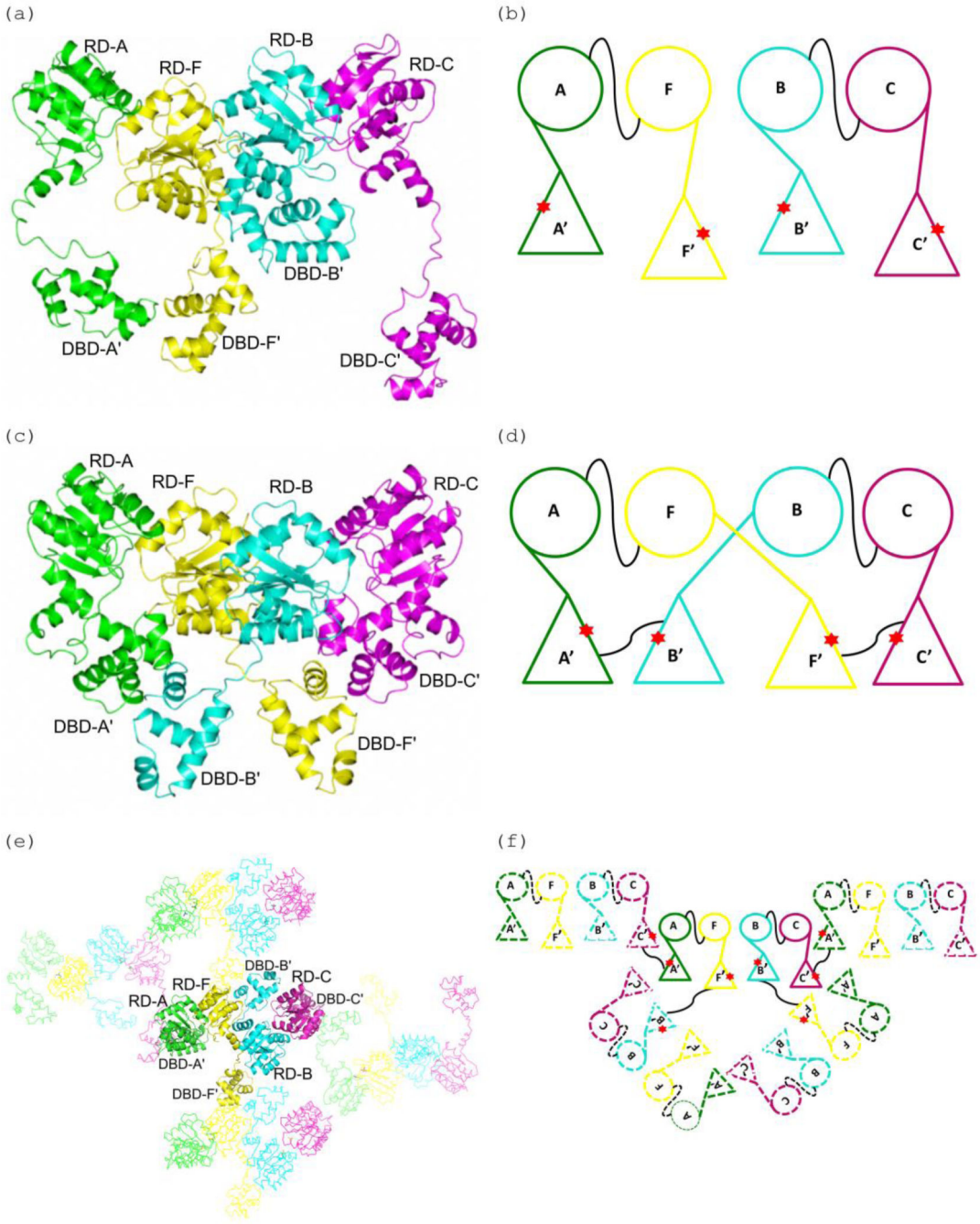

Figure 4. A comparison of the DNA domain swapping observed in the *E. faecium* LiaR and *S. aureus* VraR structures

(a), (b) Cartoon depiction of the *Efm* LiaR structure (PDB ID: **5HEV**) showing the receiver domain (RD) and DNA-binding (DBD) domains arrangements in the asymmetric unit. In the presence of BeF_3^- the crystal contained four protomers of LiaR in the asymmetric unit: A (green), F (yellow), B (cyan) and C (magenta). The star (red) identifies the dimerization interfaces of the DNA-binding domains. Two LiaR protomers (A-F and B-C) form a dimer

through dimerization of their receiver domains. The thin black line connecting the monomers identifies the dimerization interfaces of the RDs of two protomers (A-F and B-C). (c), (d) Cartoon representation of the domain swapped arrangement in the *S. aureus* VraR activated structure (PDB ID: **4IF4**). Two VraR protomers form a dimer through dimerization of their receiver domains (A-F and B-C), while the DNA binding domains form homodimers with a DNA binding domain contributed from a different receiver domain (A'-B' and F'-C') resulting in a swapping of domains. The thin black line connecting the monomers identifies the dimerization interfaces.

(e), (f) Cartoon representation of the domain swapping arrangement for the *Efm* LiaR activated structure (PDB ID: **5HEV**). Unlike VraR, the *Efm* LiaR DNA binding domains make dimer contacts to symmetry related DNA binding domains contributed by other receiver domain pairs. While this arrangement of swapped domains might be an artifact of crystallization it also demonstrates the flexibility of the DNA binding domains in the activated state. The thin black line connecting the monomers identifies the dimerization interfaces.

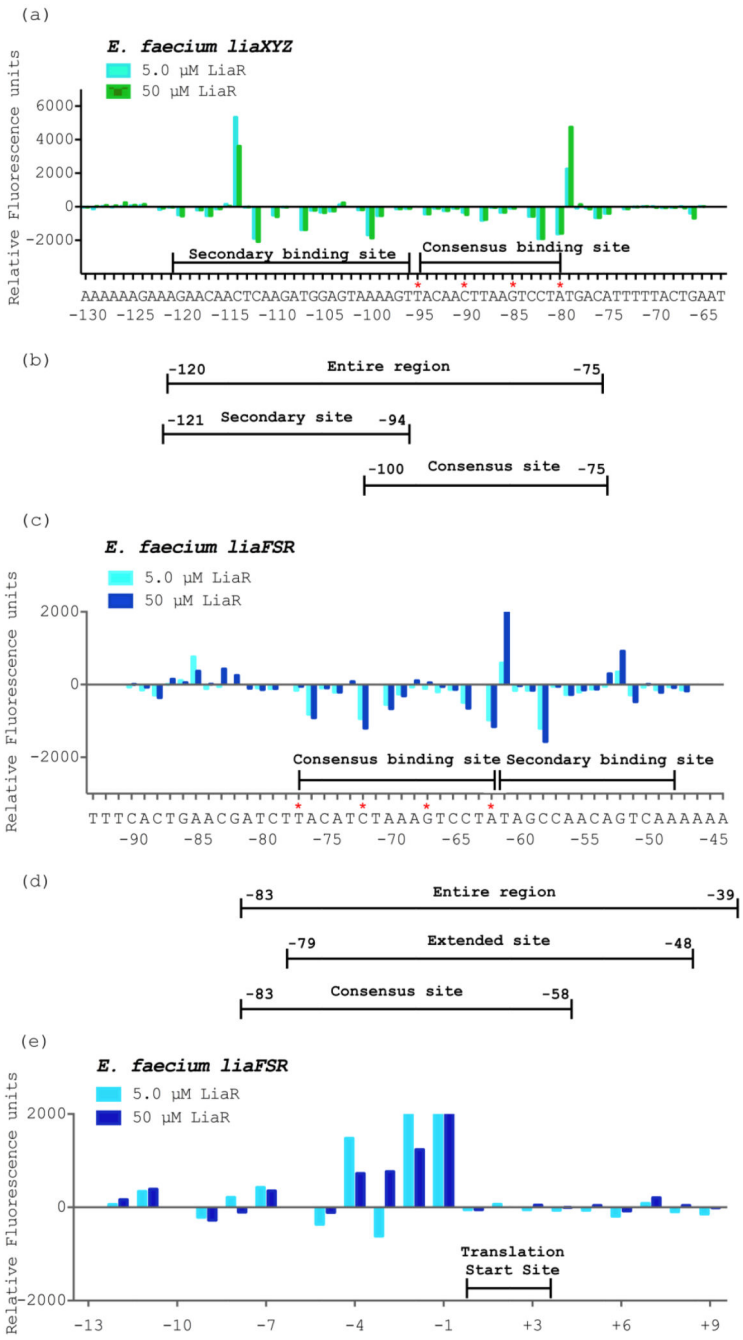

Figure 5. *Efm* LiaR recognizes complex upstream regulatory regions that extend beyond the predicted consensus sequence

DNase I Footprinting followed by Automated Capillary Electrophoresis (DFACE) was used to establish the *Efm* LiaR binding footprint within the upstream regions of the *liaXYZ* (−292 to +65) and *liaFSR* (−281 to +98) operons of *E. faecium* R494. Protection studies were performed at 0.5, 5 and 50 µM LiaR activated with the BeF_3^-. DNaseI digestion patterns are shown as histograms (a, c, e) where negative changes in relative fluorescence units indicate regions of protection and positive changes indicate hypersensitivity. All DNaseI sensitivity data are relative to a no protein negative control.

(a) *Efm* LiaR binding to the promoter region of the *liaXYZ* operon. Nucleotide positions refer to the region of LiaR binding (−120 to −75) on the DNA relative to the translation start site of LiaX (cyan, 5 μM LiaR; green, 50 μM LiaR).
(b/d) Oligonucleotides used for DNA binding studies (Table 2).
(c) *Efm* LiaR binding to the promoter region of the *liaFRS* operon. Nucleotide positions refer to the region of LiaR binding (−77 to −48) on the DNA relative to the translation start site of LiaF (cyan, 5 μM LiaR; blue, 50 μM LiaR).
(e) Superimposed electropherograms showing a strong and consistent hypersensitive site at positions −4 to −1 (AGCG) relative to the translation start site of LiaF in the presence of *Efm* LiaR (cyan, 5 μM LiaR; blue, 50 μM LiaR).

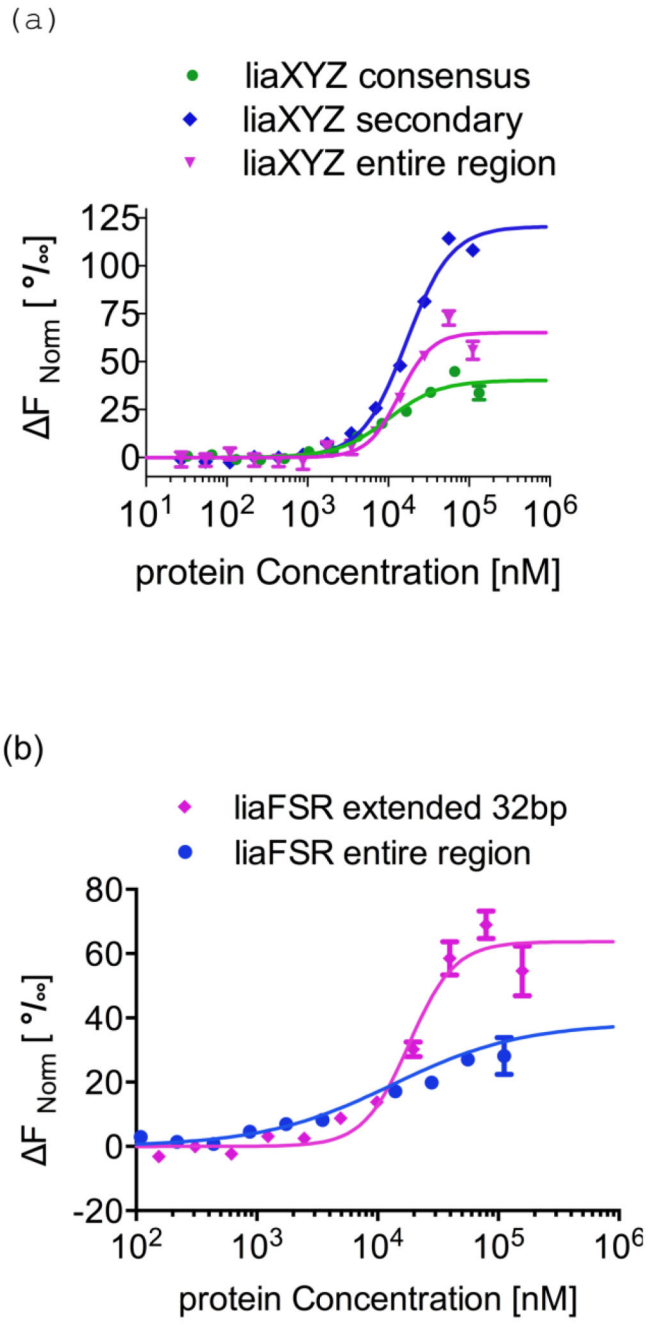

Figure 6. Adaptive mutant LiaR^{W73C} that confers increased daptomycin resistance in *E. faecium* binds more tightly to DNA binding sites within the *liaXYZ* operon

MicroScale Thermophoresis (MST) was used to measure the strength of *Efm* LiaR–DNA interactions. To determine the K_d, increasing concentrations of *Efm* LiaR^{W73C} was added to 40 nM of fluorescently labeled DNAs (Supplementary Information). F_{norm} was plotted on the y-axis in per mil [‰] unit (meaning every 1000) against the total concentration of the titrated partner on a log10 scale on the x-axis [45]. The resulting K_d values based on average from four independent MST measurements. Bars indicate the SEM (standard error of the mean)

(a) The binding of LiaR^{W73C} to the consensus (green circles), secondary (blue diamonds), or entire protected region (magenta triangles) sequences within the *liaXYZ* operon. The DNA sequence for the entire protected region is shown in Figure 5b.
(b) The binding of LiaR^{W73C} to the extended (32 bp, magenta diamonds) or entire (blue circles) protected regions of the *liaFSR* operon. The DNA sequence for the entire protected region is shown in Figure 5d.

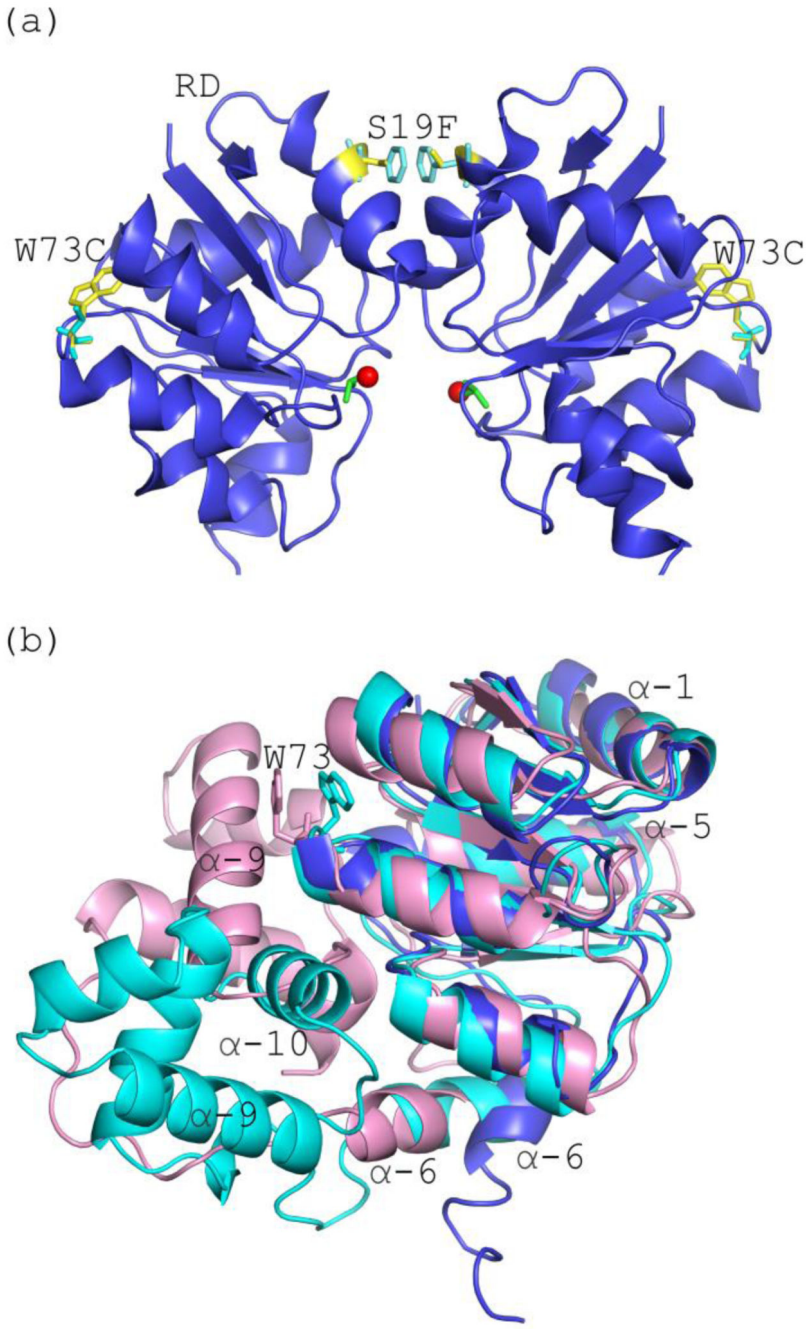

Figure 7. Mutations associated with daptomycin resistance are located within the receiver domain

(a) Expanded view of the *Efm* LiaR receiver domains showing the positions of the mutations W73C and S19F. The S19F mutation (yellow/cyan sticks) is within the dimerization interface, while the adaptive mutation W73C (yellow/cyan sticks) is not located within the molecular surfaces that comprise the LiaR dimer: (b) Structural alignment of the activated *Efm* LiaR receiver (blue) compared to the inactive state structures of VraR/NarL receiver domains (cyan/light pink). Position 73 in the VraR and NarL structures are depicted as sticks (cyan/light pink, respectively).

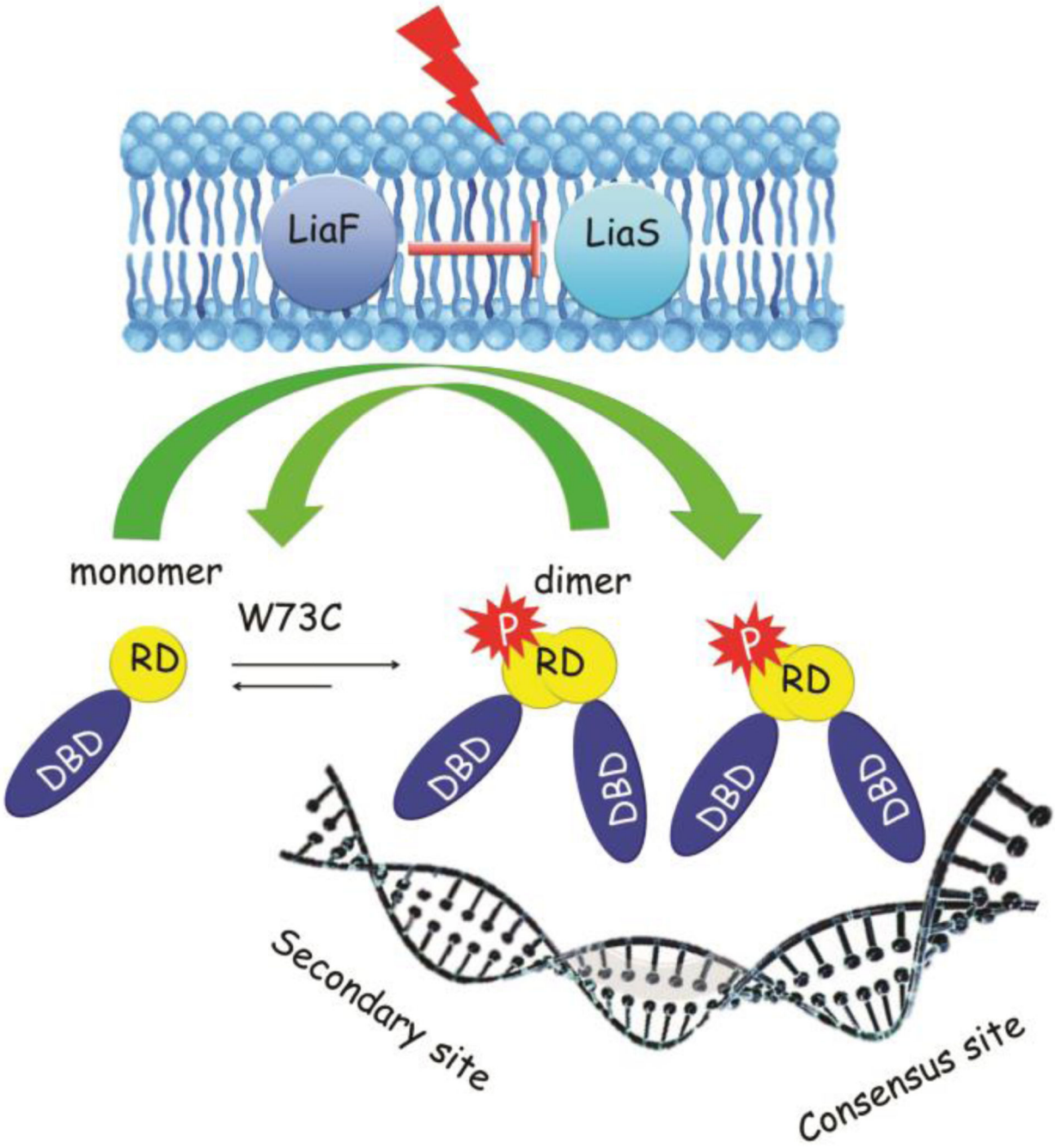

Figure 8. Adaptive mutations in *E. faecium* LiaR that have been identified during antibiotic selection

In the absence of the cell membrane acting antibiotics or membrane stress, the three-component regulatory system, LiaFSR, is turned "OFF." LiaF is thought to down regulate the kinase activity of LiaS. Typically, LiaR is phosphorylated in response to membrane stress to regulate downstream target operons. *E. faecium* LiaR is present largely as a monomer at physiologically relevant concentrations. Phosphorylation may induce changes in the conformation of the receiver domain leading to release of DNA binding domain and promoting a self-dimerization event to form an active tetramer able to bind extended DNA

sequences. The adaptive mutation W73C, even in the absence of phosphorylation, promotes a phosphorylation-like self-dimerization event that increases LiaR affinity for upstream regulatory regions. (RD - receiver domain, DBD - DNA binding domain)

Table 1

Dimerization affinities of *E. faecium* LiaR and variants in the absence and presence of BeF_3^-.

Protein name	BeF_3^-	Dimerization K_d (μM)	95% confidence intervals (μM)
LiaR	−	No dimer observed	$K_d > 1600$
LiaR	+	15	$12 < K_d < 19$
$LiaR^{W73C}$	−	182	$119 < K_d < 311$
$LiaR^{W73C}$	+	236	$82 < K_d < 1000$
$LiaR^{RD}$	−	676	$497 < K_d < 986$
$LiaR^{RD}$	+	3.4	$3.2 < K_d < 4.2$
$LiaR^{RD(W73C)}$	−	94	$70 < K_d < 128$
$LiaR^{RD(W73C)}$	+	0.8	$0.4 < K_d < 1.4$
$LiaR^{DBD}$	−	0.4	$K_d < 2.0$

Table 2

DNA binding affinity of *E. faecium* LiaR

Protein	***liaXYZ* consensus K_d (μM)**	***liaXYZ* secondary K_d (μM)**	***liaXYZ* entire protected K_d (μM)**	***liaFSR* consensus K_d (μM)**	***liaFSR* extended K_d (μM)**	***liaFSR* entire protected K_d (μM)**	**Random K_d (μM)**
$LiaR^{W73C}$	9.9±0.6	16.7±0.4	13.7±1.3	>100	18.2±1.1	13.3±1.3	>200
LiaR	N/D[a]	N/D[a]		N/D[a]			
$LiaR^{DBD}$	N/D[a]	N/D[a]		N/D[a]			

[a] no detectable binding my MST up to 450 μM LiaR, 320 μM $LiaR^{DBD}$

Table 3

Data collection and refinement statistics

Data collection	
Wavelength (Å)	0.97872
Resolution (Å)[a]	50.0-3.2 (3.26-3.2)
Space group	$P3_1$
Molecules per a.u.	4
Cell dimensions a,b,c; (Å); α, β, γ; (°)	68.03×68.03×276.95; 90×90×120
Reflections Unique[a]	23488
Average redundancy[a]	3.5 (2.9)
Completeness (%)[a]	98.3 (97.9)
R_{merge} (%)[a,b]	11.5 (0.83)
Output <I/sigI>[a]	10.1 (1.22)
Refinement	
R_{work} (%)[c]	21.86
R_{free} (%)[d]	27.04
r.m.s.d.[e] from ideality	
Bonds (Å)	0.003
Angles (°)	0.569
Wilson B-factor (Å^2)	57.6
Average B, all atoms (Å^2)	53.0
Average B, ligand, BeF_3^- (4) (Å^2)	42.5
Ramachandran[f]	
Favored (%)	97.10
Allowed (%)	2.90
Outliers (%)	0.00
PDB ID	5HEV

[a]Values for the last shell are in parenthesis

[b] $R_{merge} = \Sigma|I - \langle I \rangle| / \Sigma I$, where I is measured intensity for reflections with indices of hkl

[c] $R_{work} = \Sigma||F_O| - |F_C|| / \Sigma|F_O|$ for all data with $F_O > 2\sigma(F_O)$ excluding data to calculate R_{free}

[d] $R_{free} = \Sigma||F_O| - |F_C|| / \Sigma|F_O|$ for all data with $F_O > 2\sigma(F_O)$ excluded from refinement.

[e] Root mean square deviation